

Review

# Review of Orbital Magnetism in Graphene-Based Moiré Materials

Priyamvada Jadaun <sup>1,2,\*</sup>  and Bart Soreé <sup>1,2,3</sup> <sup>1</sup> Interuniversity Microelectronics Centre (IMEC), Kapeldreef 75, 3001 Leuven, Belgium<sup>2</sup> Department of Electrical Engineering, KU Leuven, Kasteelpark Arenberg 10, 3001 Leuven, Belgium<sup>3</sup> Department of Physics, University of Antwerp, Groenenborgerlaan 171, 2020 Antwerp, Belgium

\* Correspondence: priyamvada@utexas.edu

**Abstract:** Recent years have seen the emergence of moiré materials as an attractive platform for observing a host of novel correlated and topological phenomena. Moiré heterostructures are generated when layers of van der Waals materials are stacked such that consecutive layers are slightly mismatched in their lattice orientation or unit cell size. This slight lattice mismatch gives rise to a long-wavelength moiré pattern that modulates the electronic structure and leads to novel physics. The moiré superlattice results in flat superlattice bands, electron–electron interactions and non-trivial topology that have led to the observation of superconductivity, the quantum anomalous Hall effect and orbital magnetization, among other interesting properties. This review focuses on the experimental observation and theoretical analysis of orbital magnetism in moiré materials. These systems are novel in their ability to host magnetism that is dominated by the orbital magnetic moment of Bloch electrons. This orbital magnetic moment is easily tunable using external electric fields and carrier concentration since it originates in the quantum anomalous Hall effect. As a result, the orbital magnetism found in moiré superlattices can be highly attractive for a wide array of applications including spintronics, ultra-low-power magnetic memories, spin-based neuromorphic computing and quantum information technology.

**Keywords:** two-dimensional materials; van der Waals materials; spintronics; magnetism; topology; moiré materials; orbital magnetism; anomalous Hall effect; Chern insulators



**Citation:** Jadaun, P.; Soreé, B. Review of Orbital Magnetism in Graphene-Based Moiré Materials. *Magnetism* **2023**, *3*, 245–258. <https://doi.org/10.3390/magnetism3030019>

Academic Editors: Xichao Zhang, Israa Medlej and Roberto Zivieri

Received: 4 December 2022

Revised: 1 May 2023

Accepted: 2 June 2023

Published: 28 August 2023



**Copyright:** © 2023 by the authors. Licensee MDPI, Basel, Switzerland. This article is an open access article distributed under the terms and conditions of the Creative Commons Attribution (CC BY) license (<https://creativecommons.org/licenses/by/4.0/>).

## 1. Introduction

Moiré superlattices in heterostructures of van der Waals materials have emerged as a powerful platform for the design and exploration of novel material physics. These are materials in which successive layers of 2D materials show a slight mismatch between their lattice constants or lattice orientations. This mismatch between lattices gives rise to a long-wavelength moiré pattern that modulates the overall electronic structure and leads to the emergence of superlattice minibands within a smaller Brillouin zone. Figure 1 depicts the schematic of a moiré material, i.e., twisted bilayer graphene (Figure 1b), the mini Brillouin zone of the moiré lattice (Figure 1c), the moiré pattern in real space (Figure 1d) and the superlattice minibands (Figure 1e).

In 2010, it was discovered that introducing a rotational twist between the crystal orientations of two graphene layers stacked atop one another can drastically change the electronic properties of the material [1]. In 2016, accurate control of this twist angle was realized [2], resulting in a precisely engineered moiré superlattice. In 2011, the moiré superlattice of magic-angle-twisted bilayer graphene (TBG), in which one monolayer graphene sheet is stacked on top of another with a relative twist angle of approx.  $1^\circ$ , was predicted to host “flat” bands of  $\sim 10$  meV bandwidths with zero velocity at certain magic angles [3] (shown in Figure 1e), which was substantiated by subsequent theoretical studies [4,5]. Since then, a plethora of studies on moiré superlattices have shown the

emergence of an array of novel electronic properties. Table 1 lists different types of moiré structures, their material realizations and their properties.

**Table 1.** Table detailing a list of moiré materials and their properties.

Moiré Type	Moiré Material	Model	Moiré Properties
Twisted graphene homobilayer	Twisted bilayer graphene	Two-orbital extended Hubbard model [6]	Mott insulation [7]; superconductivity [8]; correlated quantum anomalous Hall (QAH) insulator [9]
Twisted transition metal dichalcogenide (TMD) homobilayers	Twisted bilayer MoS <sub>2</sub> ; MoSe <sub>2</sub>	Asymmetric px–py Hubbard model [10]	Nematic (anti)ferromagnets [10]
	Twisted bilayer WS <sub>2</sub> , WSe <sub>2</sub>	Hubbard model [11]	Correlated insulator [12]
	Twisted bilayer WTe <sub>2</sub>	Inverted band insulator; strong spin-orbit coupling [11]	Quantum spin Hall insulator; fractional Chern/topological insulator [11]
Twisted graphene heterobilayer	Graphene/hexagonal boron nitride (hBN)	Two-orbital extended Hubbard model [6]	Mott insulation [7]; superconductivity [8]; correlated QAH insulator [9]
Twisted TMD heterobilayers	Twisted heterostructures of MoS <sub>2</sub> , WS <sub>2</sub> , and WSe <sub>2</sub>	Doped multi-orbital Hubbard models [11]	Moiré excitons [13,14]
	Twisted WS <sub>2</sub> /WSe <sub>2</sub> heterostructures	Hubbard model [11]	Correlated insulator [12]; Wigner crystals [15]
Twisted graphene multilayers	Twisted double bilayer graphene	Two-orbital extended Hubbard model [11]	Ferromagnetic insulator superconductivity [16,17]
	Aligned ABC trilayer graphene on boron nitride	Honeycomb	Correlated Chern insulator [18]; Orbital magnetism [19]
	Twisted monolayer-bilayer graphene	Honeycomb	Quantized anomalous Hall effect and electrically tunable magnetism [20]
Twisted TMD multilayers	Twisted double bilayers of WSe <sub>2</sub> 110	Hubbard model [11]	Correlated insulator [12]

Moiré materials can be designed with specific values of interlayer rotational alignment such that the lowest energy bands develop bandwidths that are significantly smaller than the native scale of electron–electron interactions. The physical origin of these “flat” moiré bands lies in the localization of electrons by the periodic moiré lattice potential.

The dominant interactions in these flat moiré bands are electron–electron correlations due to the reduced kinetic energy of electrons [21], resulting in the appearance of “correlated insulator” states. These have been experimentally observed at integer electron or hole filling of the moiré unit cell, resulting from the interaction-induced breaking of one or more of the spin, valley, or lattice symmetries [22]. Experimental realizations have also been made at fractional fillings of bands in TBG with a moiré twist angle of  $\sim 1.1^\circ$  [7,23], ABC-trilayer graphene/hBN [24,25] twisted double-bilayer graphene systems (TDBG) [16,26–29] and moiré WSe<sub>2</sub> [12].

Moiré materials also demonstrate novel topological states. For instance, TBG was theoretically predicted to host fragile topology [30,31] and was experimentally shown to demonstrate Hofstadter spectra at strong magnetic fields [32,33]. One of the topological states of interest is the quantized anomalous Hall effect [34], which occurs in two-dimensional insulators whose bands have finite net Chern numbers and requires broken time-reversal symmetry. In graphene-based systems, Chern bands arise innately upon the breaking of sublattice symmetry, which results in a massive Dirac spectrum [20]. However, in systems without electron correlations, bands from the two inequivalent valleys at opposite corners

of graphene's hexagonal Brillouin zone are required by time-reversal symmetry to acquire equal and opposite Chern numbers, resulting in a net zero Chern number. In graphene-based moiré superlattices, the superlattice bands can inherit the non-zero Chern numbers that originate in the Berry curvature of the monolayer graphene Dirac points [35,36]. For certain twist angles, as the superlattice bands become flat, electron correlations become relatively dominant and lead to symmetry breaking which results in an observable QAH state with a finite net Chern number. This state is manifested primarily as resistivity peaks at integer fillings of normally fourfold degenerate superlattice bands [3,24]. Figure 2 shows experimental results demonstrating a QAH state in TBG aligned to hexagonal boron nitride with  $\theta \approx 1.15 \pm 0.01^\circ$  and with filling factor  $\nu = 3$ , as reported in ref. [37].

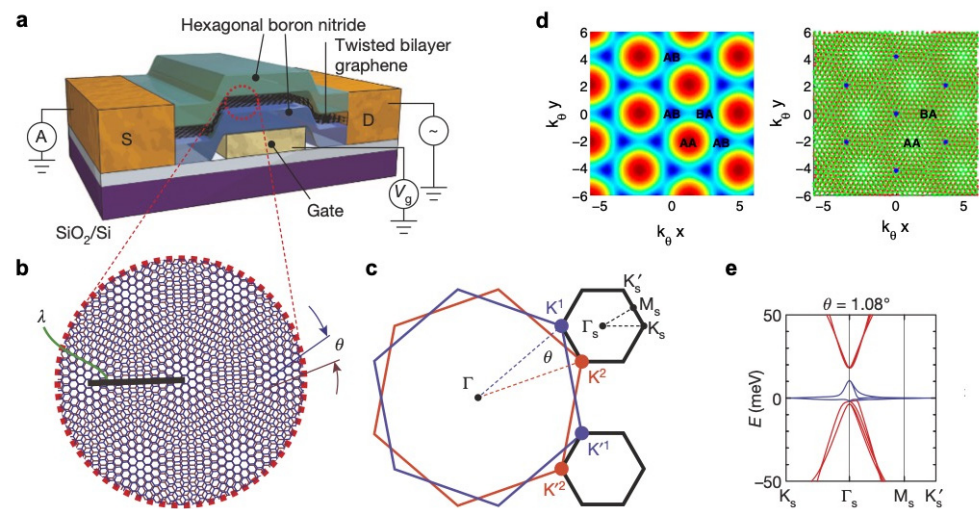


**Figure 1.** Schematic of the moiré pattern and the electronic structure. (a) Schematic of a TBG device. The TBG forms the device channel and is fabricated on a  $\text{SiO}_2/\text{Si}$  substrate with hBN as a capping layer.  $S$  and  $D$  label the source and drain, respectively, and  $V_g$  represents the gate voltage. Conductance of the device is measured while varying  $V_g$ . (b) Schematic of the moiré twist between graphene layers with twist angle  $\theta$  and moiré wavelength  $\lambda = a/[2\sin(\theta/2)]$ , where  $a = 0.246$  nm is the lattice constant of graphene. (c) The mini Brillouin zone of the TBG which is constructed from the difference between  $K^1$  and  $K^2$  (or  $K'^1$  and  $K'^2$ ), where  $K^1$  and  $K^2$  form the wavevectors for the individual graphene layers comprising TBG. (d) Moiré pattern in TBG, with stacking regions (AA, AB and BA) marked. Distances are measured in units of  $k_\theta^{-1}$ , with  $k_\theta = 2k_D \sin(\theta/2)$ ,  $k_D$  being the Dirac wave vector. (e) Electronic structure of magic-angle TBG with ( $\theta = 1.08^\circ$ ), calculated using an ab initio tight-binding method. The flat bands are shown in blue. Panels (a–c,e) are taken from ref. [7], and (d) is taken from ref. [3].

In addition to demonstrations of the QAH state, the spontaneous breaking of time-reversal symmetry [38–44] has also been reported to result in orbital ferromagnetism in TBG aligned to hBN [9,37], rhombohedral trilayer graphene also aligned to hBN [18] and twisted monolayer-bilayer graphene (tMBG) [20,45]. In contrast to magnetically doped topological insulators in which the quantum anomalous Hall effects originates in the large spin–orbit coupling of topological insulators, graphene moiré systems have negligible spin–orbit coupling, and thus the magnetism in these moiré systems is thought to be primarily orbital, causing these systems to be labeled “orbital Chern insulators” [20].

Built from layers of two-dimensional materials, moiré materials demonstrate high degrees of control and tunability of their properties. For instance, in graphene-based moiré heterostructures, the band topology can be designed by varying the number of graphene layers and the details of the external environment, such as the neighboring crystals [45].

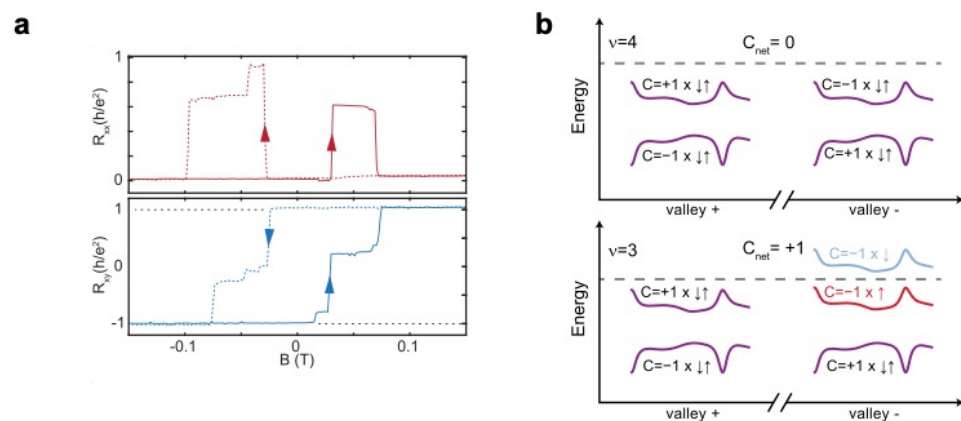


**Figure 2.** Experimental results on the quantized anomalous Hall effect in twisted bilayer graphene at 1.6 K. (a) Plot of the Hall resistance  $R_{xx}$  and  $R_{xy}$ , plotted while the external magnetic field at  $B$  is swept, keeping  $n = 2.37 \times 10^{12} \text{ cm}^{-2}$ , with the sweep direction shown in arrows. The figure shows the switching of Hall resistivity between  $+1$  and  $-1$  as the external magnetic field is changed. (b) Schematic of the moiré band structure at full filling of a moiré unit cell,  $\nu = 4$  (above) and  $\nu = 3$  (below). A net Chern number of 1 is observed at  $\nu = 3$  which accounts for the quantized anomalous Hall effect shown in (a). Figure is adapted from ref. [37].

Recent years have seen a multitude of reviews on moiré materials that comprehensively cover a range of moiré systems and discuss their fabrication techniques [46], present a brief overview of their novel properties [47] and discuss moiré pattern-modified electrical properties [48] and electronic and excitonic properties in moiré systems [49]. In contrast, this review focuses on the recently discovered orbital magnetism in moiré materials, especially in graphene-based moiré systems. This review paper is structured as follows. Section 2 describes experimental discoveries pertaining to orbital magnetization in moiré heterostructures, Section 3 details the theoretical studies of the same, and Section 4 discusses possible technological applications of orbital magnetization as well as future research directions.

## 2. Experimental Discovery of Orbital Magnetism

Orbital magnetization in crystals arises from the Berry curvature of the bands and the orbital angular momentum of the Bloch electron wave packet [50]. While orbital magnetization was known to contribute to total magnetism in materials, ferromagnetism typically also included contributions from the electron spin [22]. Ferromagnetism was recently reported in TBG over a range of carrier densities around  $3/4$  filling of the conduction band [9,37]. Additional experiments on hysteretic transport in moiré heterostructures composed of graphene and hexagonal boron nitride [18,20,45] also point to ferromagnetic order in these materials, despite none of these materials being intrinsically magnetic. The negligible spin-orbit coupling rules out contributions from the spin angular momentum of electrons. Therefore, these results are thought to demonstrate the emergence of purely orbital ferromagnetism in moiré materials [38–44,51].

In general, magnetism in materials is composed of two components, i.e., the spin and the orbital contributions [52]. While the spin magnetic moment originates in the electron spin quantum number, the orbital magnetic moment arises from the Berry curvature of the Bloch bands and the orbital angular momentum of the Bloch electron wave packet [50]. In general, ferromagnets have nonzero contributions from both spin and orbital magnetism. In most ferromagnets, the spin magnetic contribution is dominant, and magnetism is predominantly a result of spontaneous spin alignment driven by exchange interactions. This alignment breaks spin rotational invariance and leads to a nonzero, spatially averaged spin moment density [53]. For most ferromagnets, in comparison to the dominant spin contribution, orbital magnetism plays a secondary role and acts as a small, parasitic contribution to magnetization from orbital currents [53]. As a result of its dominant presence, spin magne-

tization has been extensively studied and is relatively well understood [52]. In contrast, the study of orbital magnetization, called the modern theory of orbital magnetization, is relatively new [50,54]. Both spin and orbital magnetization can be measured separately using magnetomechanical [55] or magnetic circular dichroism measurements [56]. The conditions for hosting a purely orbital ferromagnetic order include the presence of a time-reversal symmetric electronic degree of freedom in addition to strong electron correlations, while a spin magnetic order does not require the presence of electron correlations [22]. When comparing the magnitudes of magnetization densities observed from spin and orbital contributions, the magnetization density ( $m$ ) of one orbital moment per superlattice cell is reported to be  $m \lesssim 0.1 \mu_B/\text{nm}^2$  for ABC trilayer graphene/hexagonal boron nitride [18] (where  $\mu_B$  is the Bohr magneton and  $\mu_B \approx 0.06 \text{ meV/T}$ ). This magnetization density is more than three orders of magnitude smaller than that seen in typical spin-based magnetic systems [22]. Finally, while electric field control of spin-based magnetism is difficult to achieve, electric control of orbital magnetism in moiré materials is relatively straightforward, with multiple experimental reports of the same, for instance the electric-field-induced reversal of the magnetic state shown in tMBG [20].

### 2.1. Twisted Bilayer Graphene

Orbital ferromagnetism was initially reported in TBG at 3/4 filling of the conduction band accompanied by a giant anomalous Hall (AH) effect that displayed hysteresis in the magnetic field, with the hysteretic anomalous Hall effect as large as 10.4 k $\Omega$  [9]. The study thus suggested that at 3/4 filling, TBG is a correlated Chern insulator. In addition to the novel properties observed at 3/4 filling, the study also showed high resistance states at 1/4 and 1/2 fillings of the moiré Brillouin zone (mBZ) that correspond to one and two electrons per superlattice unit cell, respectively. These states had been previously attributed to correlated insulating states [8,23].

Later measurements demonstrated the presence of a quantum anomalous Hall state in TBG with a longitudinal resistivity of 10  $\Omega$  [37]. This was shown to be a Chern insulator with a Chern number of 1 at 3/4 filling [37]. Subsequent measurements with a superconducting quantum interference device (SQUID) reported the value of orbital magnetization to be approximately 2–4 Bohr magnetons per moiré unit cell [22]. Figure 3 shows experimental images of orbital magnetization in TBG at 2.1 K, measured using spatially resolved SQUID magnetometry [22]. This value is markedly larger than the expected spin contribution of 1 Bohr magneton per moiré unit cell, suggesting a strong orbital component to the total magnetization [21]. Additionally, magnetization in TBG is observed to be highly anisotropic, which can be explained by the electron currents circulating in-plane of the orbital magnet [21]. This result also precludes a strong spin contribution to magnetization as the latter is isotropic and spin–orbit coupling in graphene is very small.

Importantly, these experiments also showed that the orbital magnetization can be switched by driving very small DC currents (ranging from 10 to 50 nA) through the TBG samples [9,37]. The current required for switching magnetization is orders of magnitude smaller than the current used in spin torque devices today [57]. The mechanism for this highly efficient current-driven magnetization reversal was presented in [58]. Here, the authors note that in magic-angle TBG, due to the large Berry curvatures of the flat moiré superlattice bands, the orbital magnetic moments carried by the Bloch electrons can be quite large (~tens of Bohr magnetons per electron). Additionally, the breaking of symmetry from the neighboring hBN layer allows for a small, externally applied electric current to induce a large orbital magnetization. This induced orbital magnetization then couples with the bulk magnetization of the TBG sample, facilitating energy-efficient electrical control of magnetization [58].

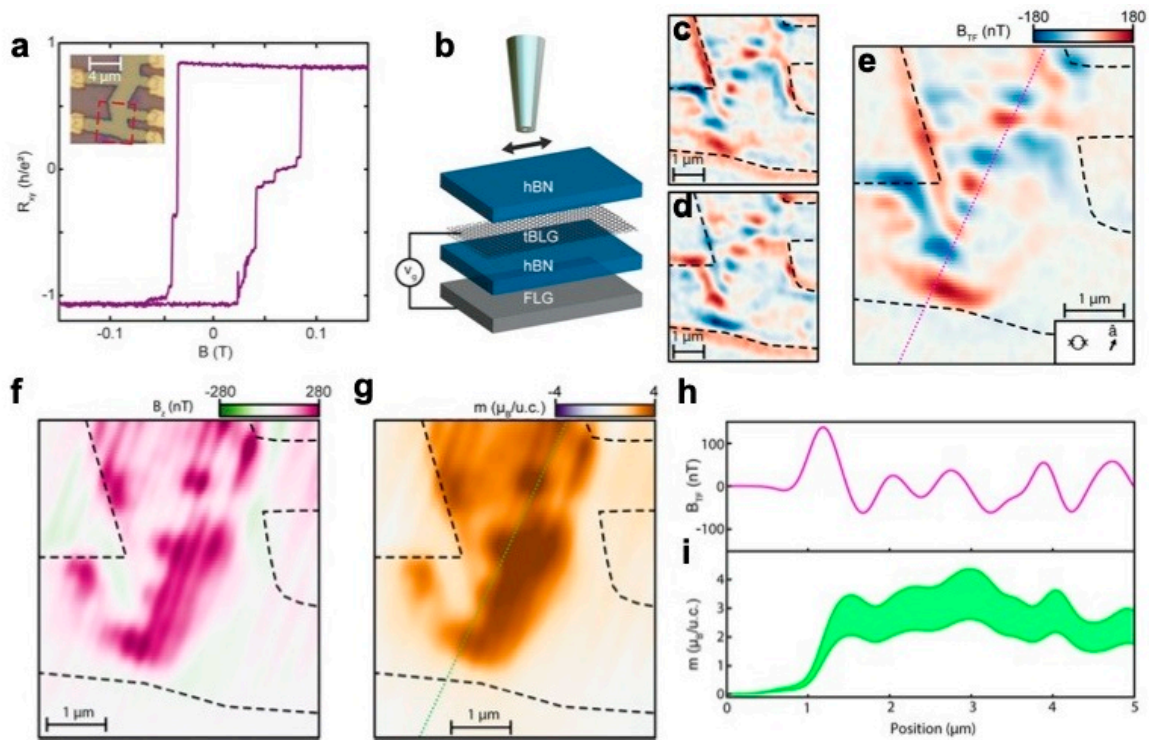


**Figure 3.** Imaging orbital magnetization in TBG. (a) Hall resistance at  $T = 2.1$  K of a TBG device aligned to hexagonal boron nitride measured with electron density  $n = 2.36 \times 10^{12} \text{ cm}^{-2}$ . Inset: optical micrograph of the TBG device with the scanned region outlined in red. (b) Schematic of the experimental setup for imaging the orbital magnetization using spatially resolved SQUID magnetometry. A nanoscale indium SQUID with diameter  $d = 215$  nm is placed above the plane of TBG at a height of  $h \approx 140$  nm. The SQUID is coupled to a quartz tuning fork, and the former's response is measured at frequency  $B_{TF} \approx \hat{a} \cdot \nabla_r B_z$ , where  $B_z$  represents the static magnetic field and  $|\hat{a}| \approx 189$  nm is the tuning fork oscillation amplitude. (c,d)  $B_{TF}$  measured using  $B = 22$  mT after field training to (c) +200 mT and (d) −200 mT. (e) The gradient magnetometry signal originating in the fully polarized orbital ferromagnet, obtained by taking the difference in data from (c) and (d) to remove magnetic contributions from electric fields and thermal gradients. Color scale for (c–e) is shown above panel (e). (f) The static out-of-plane magnetic field  $B_z$ , calculated by integrating data in (e). (g) Magnetization density  $m$ . Data are plotted in units of Bohr magnetons per moiré unit cell area  $A \approx 130 \text{ nm}^2$ . (h) Magnetic field BTF and (i) magnetization  $m$  plotted along the indicated contours in (e,g). Figure is adapted from ref. [22].

Further examination of the orbital magnetic state in TBG for a twist angle of  $\theta \sim 1.68^\circ$  showed that the orbital magnetic moment was generated by the moiré-scale current loops in the Chern insulator state [59]. In the presence of external magnetic fields, the study reported a large and linear response of valley splitting arising from the coupling of the large orbital magnetic moment induced by chiral current loops with the magnetic field. The orbital magnetic moment was reported to be about  $10.7 \mu\text{B}$  per moiré supercell [59].

## 2.2. Aligned ABC Trilayer Graphene on Boron Nitride

Reports of orbital magnetization in TBG inspired further examination of other members of the family of moiré heterostructures. Among these, ABC trilayer graphene aligned to a hexagonal boron nitride (ABC-TLG/hBN) moiré superlattice attracted particular interest because it features nearly flat moiré minibands with a valley-dependent and electrically tunable Chern number [35,60]. The authors of [18] reported the experimental observation of a correlated Chern insulator in an ABC-TLG/hBN moiré superlattice. For  $1/4$  filling of the superlattice bands, which corresponds to one hole per moiré unit cell, the Hall resistance

was quantized at  $h/2e^2$  (where  $h$  is Planck's constant and  $e$  is the charge on the electron), indicating the Chern number  $C = 2$  for an external magnetic field exceeding 0.4 Tesla. The correlated Chern insulator was found to persist to zero magnetic field, spontaneously breaking the time-reversal symmetry and generating valley-flavor ferromagnetism at  $1/4$  filling. This orbital ferromagnetic state exhibited considerable magnetic hysteresis and a large anomalous Hall signal at zero external magnetic field. The Chern insulator state was also tunable as reversing the direction of an applied vertical electric field switched the moiré minibands of ABC-TLG/hBN between zero and finite Chern numbers.

Expanding upon previous discoveries of Chern insulator and orbital ferromagnetic states in moiré superlattices at integer fillings, the authors of [19] recently reported ferromagnetism even at non-integer-filling (NIF) of a flat Chern band in a ABC-TLG/hBN moiré superlattice. Experimental observations showed marked hysteretic behavior with a large, anomalous Hall resistivity in a broad region of densities centered in the valence miniband at a carrier density  $n$  of 2.3 holes per moiré unit cell [19]. This remarkably large, anomalous Hall signal could be tunable not only in magnitude but also in sign by altering the carrier density and the displacement field. The observed high anisotropy of the ferromagnetic state indicates that it is likely purely orbital in character [19]. The authors explained their observations by proposing either an incipient Chern insulator state or a conductive orbital ferromagnetic state [19].

### 2.3. Twisted Monolayer-Bilayer Graphene

Among graphene-based moiré heterostructures, tMBG is known to be a particularly rich system due to its low crystal symmetry and the tunability of its bandwidth using an external electric field [61].

The tMBG moiré consists of a triangular lattice of ABB-stacked regions interspersed with more structurally stable ABA and ABC regions, with the wavefunctions of the low-energy bands localized near the ABB regions [20]. For a twist angle of  $\theta = 1.25^\circ$ , the authors of [20] reported a QAH with the emergence of a single spin- and valley-polarized band at odd integer filling and Chern number  $C = 2$ . The band structure of tMBG originates in the moiré-induced hybridization of the monolayer graphene Dirac cone with the parabolic low-energy band of bilayer graphene [17]. At fillings of 1 and 3 electrons per moiré unit cell, the authors of [20] observed a quantized anomalous Hall effect with transverse resistance approximately equal to  $h/2e^2$ , indicating the spontaneous polarization of the system into a single-valley-projected band with a Chern number  $C = 2$  [20].

At a filling of 3 electrons per moiré unit cell, the quantum anomalous Hall effect was found to be tunable such that its sign could be reversed via field-effect control of the chemical potential. This transition was also found to be hysteretic and was used to demonstrate a non-volatile electric-field-induced reversal of the magnetic state [20]. The authors note that tMBG, in contrast to TBG and rhombohedral trilayer graphene, does not rely on precise alignment to hBN, making it an all-carbon quantum anomalous Hall system. As most reported cases of magnetism arise predominantly from electron spin contributions, controlling magnetism with electric fields, a longstanding goal in spintronics and multiferroics [62], is a difficult proposition. The rise of electrically tunable orbital magnetism in moiré materials such as tMBG has led to major strides toward achieving this technologically impactful goal [20]. The theoretical study reported in [53] indicated that the electric field control of orbital magnetism originates from the chiral topological edge states, which drive a change in the sign of the orbital magnetization and a reversal of the magnetic state. This stands in contrast to previously observed anomalous Hall effect sign reversals [63,64] that arise from a change in the sign of the total anomalous Hall effect for the same magnetic state.

Electrical switching of orbital magnetization is shown to occur with perfect fidelity and appears to be indefinitely non-volatile at  $T = 6.4$  K [20]. The excellent reproducibility of field-effect switching that is highly useful for technological applications arises from the

absence of states with partial or intermediate valley polarization, which arises in turn from the extreme anisotropy inherent in a purely orbital two-dimensional magnet [20].

The authors of [45] reported a plethora of correlated metallic and insulating states, in addition to topological magnetic states in tMBG. When an external perpendicular electric field was applied pointing from the monolayer towards the bilayer graphene, the entire moiré system approximated that of twisted double-bilayer graphene, and the authors reported the emergence of orbital ferromagnetism at 1/4 filling of the conduction band in addition to an associated anomalous Hall effect. Here, too, this magnetization was found to be electrically tunable, such that the direction of the magnetization could be switched via electrostatic doping at zero magnetic field. When the external electric field was applied in the opposite direction, the tMBG approximated twisted bilayer graphene, and the authors reported observing correlated states that underwent an orbitally driven insulating transition above a critical perpendicular magnetic field. The demonstration of electrically tunable orbital magnetization in tMBG was interesting as it portends important applications in the field of spintronics [45].

A later study of tMBG at twist angles of  $\theta = 1.13^\circ$  and  $\theta = 1.19^\circ$  [61] did not report signatures of QAH in tMBG at odd integer band fillings under zero external magnetic field. Instead, the authors reported inter-valley coherent (IVC) states possibly competing with Ising-like valley polarized (VP) states at zero magnetic field. The application of large magnetic fields altered this competition between the states, transforming the low-energy bands into a recursive series of Hofstadter minibands [61] and resulting in multiple Chern insulator states that emerged spontaneously. These results indicate that orbital magnetism is abundant within the correlated phase diagram of tMBG [61].

### 3. Theoretical Reports on Orbital Magnetism

An initial theoretical examination of the twisted two-layer graphene system, later termed TBG, showed that the electronic structure of this system consisted of moiré Bloch bands. At certain values of the relative twist angle, the Dirac velocity vanished and the lowest moiré band flattened [3]. Electronic structure models were subsequently derived for these systems that further substantiated the prediction of the localization of electrons at certain twist angles [4]. Later, a host of theoretical studies made the prediction of ferromagnetism in TBG that originates purely in the orbital angular momentum of electrons, with negligible spin contribution [38–41,44,53,65–67]. Prior to the discovery of orbital ferromagnetism in TBG, magnetism in known materials was always thought to include contributions from the spin of electrons.

Motivated by the experimental observation of large resistance peaks at certain integer fillings of the moiré unit cell accompanied by an AH effect [9], a theoretical study examined the mechanism behind this AH effect [38]. The authors showed that the broken inversion symmetry in the TBG system aligned to hBN breaks the degeneracy of the moiré superlattice bands, leading to two Chern bands per valley. The spontaneous polarization of carriers into spin and valley states removes the remaining spin and valley symmetry, leading to an AH state at  $\nu = 3$  [38]. This was supported by the theoretical findings of [39], which provided further evidence that it was the symmetry breaking from the hBN layer aligned to TBG that gapped out the Dirac crossings in bilayer graphene and allowed for the emergence of valence and conduction bands with equal and opposite Chern numbers  $C = \pm 1$ . They explained the observation of the AH effect at 3/4 filling in terms of a spin-valley-polarized ferromagnetic insulator [39]. Subsequently, a first-principles study of compressed twisted bilayer graphene provided evidence of flat-band magnetism and half-metallicity in TBG [68]. This study showed that the band structure of TBG could be controlled by utilizing extrinsic doping, pressure and an external electric field, resulting in the emergence of spontaneous localized magnetic moments. This local magnetic ordering could be further tuned between ferromagnetism and antiferromagnetism using an external electric field [68].

As more experiments reported Chern insulator states and orbital ferromagnetism in TBG/hBN [9,37], ABC-stacked trilayer graphene/hBN [18,24,25] and TDBG [16,26,27], a

theoretical paper explored the physics of narrow moiré bands in the strong interaction limit, i.e., the limit at which the Coulomb interaction is much larger than the bandwidth [43]. Using analytical arguments and numerical calculations, including exact diagonalization (ED) and a density matrix renormalization group (DMRG), the study showed that in the strong interaction limit, when band degeneracy was broken such that the conduction and valence bands were separated from each other by energy gaps, the spinful electrons occupied two inequivalent valleys (+ and −) that could be mapped to one another via time reversal. Consequently, the study showed that the + and − valleys of the moiré band possessed equal and opposite Chern numbers. Additionally, the authors showed that in the flat-band limit, ferromagnetism was a favored state even for a topologically trivial band [43]. The presence of topology only serves to strengthen Hund’s effect, thereby making the spin-valley ferromagnetic insulator even more likely. This result was further substantiated assuming a Hubbard-like interaction in which the ferromagnetic (spin- and valley-polarized) states were found to be the ideal ground-state candidates for TBG at 3/4 filling in the perfectly flat band limit [44]. A theoretical examination of TBG at  $\pm 1/2$  filling using the all-band Hartree–Fock variational method showed the presence of valley-polarized states exhibiting a moiré orbital antiferromagnetic ordering on an emergent honeycomb lattice with a pattern constituting opposite circulating currents in the moiré supercell [40]. Figure 4 depicts these circulating currents and emergent magnetic fields for standalone TBG (Figure 4a) and TBG placed on hexagonal boron nitride (Figure 4b).

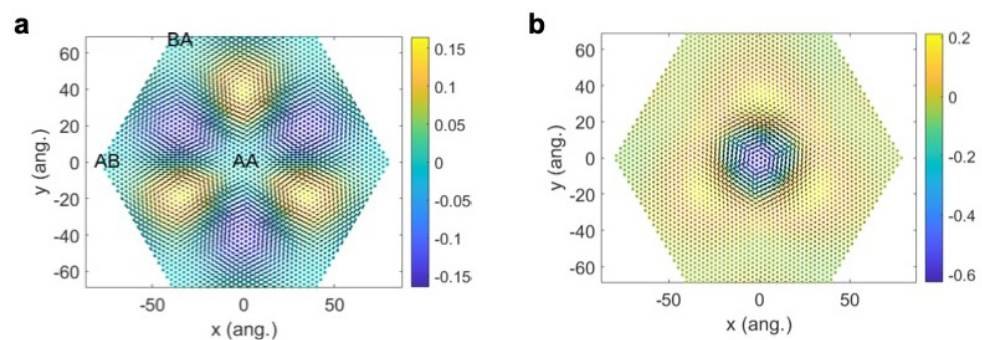


**Figure 4.** The real-space distributions of current densities and magnetic field for MATBG at 1/2 filling. (a) Current densities and magnetic field plotted for a standalone TBG layer with the staggered sublattice potential = 0. (b) Current densities and magnetic field plotted for TBG placed on hexagonal boron nitride, with staggered sublattice potential of 15 meV exerted on the bottom graphene layer. The color coding shows the strength of the magnetic field in units of Gauss. The directions and amplitudes of the current densities are shown by black arrows. Figure is taken from ref. [40]. Figure is adapted from ref. [34].

A pseudo-Landau-level representation of TBG was developed [67] which was used to study the low-energy electronic structure in the small-twist-angle limit. The study proposed that this system could be viewed in terms of 2D Dirac models under pseudo-magnetic fields generated by the moiré pattern. In such a picture, the nontrivial topology of the two low-energy bands per valley originates from the two zeroth pseudo-Landau levels (LLs) of Dirac fermions with opposite effective magnetic fields. As a result, these two zeroth LLs (for each valley) carry opposite Chern numbers ( $\pm 1$ ) and opposite sublattice polarizations. Overall, the two valleys give rise to a total of four low-energy bands (two bands per valley) that are equivalent to four zeroth pseudo-LLs [67]. Small Coulomb interactions can then split the pseudo-LL degeneracy at integer fillings, leading to insulating states with fully polarized zeroth pseudo-LLs and non-vanishing total Chern numbers. When only one out of the four zeroth pseudo LLs is occupied (empty), the TBG exhibits an insulating state with non-vanishing Chern number  $C = \pm 1$  per spin, as seen in 3/4 filled magic-angle TBG [67]. Extending this work further, recent theoretical work has proposed the emergence of fractional quantum anomalous Hall states (FQAH) in TBG/hBN at 10/3 and 17/5 band fillings in the flat-band limit [66].

The electric field tunability of orbital magnetism in moiré materials was theoretically studied using the mean-field approach and symmetry analysis [53]. The study found that in cases in which ferromagnetism mainly results from spontaneous orbital moments and not spin moments, as seen for the orbital ferromagnetic states in moiré systems, the magnetizations of weakly n-doped and weakly p-doped insulators can differ in sign in the same magnetic state characterized by the sign of the Chern number [53]. This property allows for the reversal of orbital magnetization purely through the use of an external electric field or voltage in the presence of a magnetic field. This mechanism that generates opposite signs of magnetization for n- and p-doping is closely related to the Chern insulator state itself and is therefore widely seen in the orbital ferromagnets observed in various moiré heterostructures [53]. This study also puts forth that the sublattice polarization that is crucial to the emergence of orbital magnetization in TBG can occur spontaneously or can also be forced via alignment to hBN. Spontaneous valley and spin polarizations are then energetically favored when the moiré bands are in the flat-band regime [53]. A detailed mechanism for the current-driven reversal of orbital magnetization was later proposed in [69], in which the authors proposed that both magnetic fields and transport bias voltages apply pressure to magnetic domain walls and lead to magnetization switching, which occurs along a line in the (current, magnetic field) control parameter space. The study was able to utilize conventional Landau–Lifshitz equations to capture and analyze the dynamics of domain pinning [69].

#### 4. Discussion and Future Work

Owing to the large number of correlated quantum phenomena discovered in the family of moiré systems and the tunability of their properties with external fields, moiré heterostructures have been found to be attractive for a variety of technologically important applications. Amongst these is the proposal to utilize moiré heterostructures, including their orbital magnetic phases, as a condensed matter quantum simulator [11]. Another attractive application for the orbital magnetization found in moiré heterostructures is in the field of spintronics and magnetic memories [20]. The ability to electrically control and switch magnetism is rare among known materials and is often achieved only in multiferroics; therefore, moiré systems provide a novel platform for implementing field- and carrier density-controlled magnetism, promising spintronic applications [45,58]. In TBG, the absolute magnitude of the current required to switch the orbital magnetization state ( $\sim 10^{-9}$  A) was shown to be considerably smaller than that reported in most other systems [37]. Thus, orbital magnetization in moiré heterostructures can be used to implement ultra-low-power spintronic and magnetic applications [37]. In particular, voltage control of magnetic states can be used to electrically write and manipulate non-volatile magnetic-domain structures with chiral edge states that are promising for various applications, including ultra-low-power magnetic memories and spin-based neuromorphic computing [20,70]. For instance, for TBG aligned to hexagonal boron nitride, authors reported deterministic and high-fidelity writing of a magnetic bit using 20 nA current pulses and a nonvolatile readout of the bit using the large resulting change in the anomalous Hall resistance using  $< 100$  pA of applied alternating current [37]. This results in an estimated current density  $J < 10^3$  A·cm<sup>-2</sup>, which the authors state is at least one order of magnitude smaller than that required in competing systems such as GaMnAs ( $J = 3.4 \times 10^5$  A·cm<sup>-2</sup>) [71] and Cr-(BiSb)<sub>2</sub>Te<sub>3</sub> heterostructures ( $J = 8.9 \times 10^4$  A·cm<sup>-2</sup>) [72]. The authors of [9] also reported using ultra-low current (50 nA) to switch the magnetization state in MATBG with  $\theta = 1.17^\circ$ . Similarly, the authors of [73] reported a hysteretic switching of the magnetic state in a trilayer heterostructure consisting of a MoTe<sub>2</sub> bilayer and a WSe<sub>2</sub> monolayer with a twist angle of 60 while using a switching current of 100 nA, corresponding to a current density of  $J < 10^3$  A·cm<sup>-2</sup>. Again, the ultra-low switching current used in this case was at least one order of magnitude smaller than what is required in competing systems that allow for in situ electrical readout. Thus, experimental reports repeatedly show ultra-low-power electric control of the orbital magnetic state in moiré heterostructures, indicating the exceptional promise of moiré materials

for ultra-low-power spintronic and magnetic applications [37]. The experimental realization of magnetic skyrmions in moiré heterostructures, as predicted in [74], can open up novel pathways for the implementation of advanced spintronic neuromorphic computing devices [75].

Even when restricted to low temperatures, the gate-switchable chirality of orbital Chern insulators could be used as the central element in reconfigurable and compact microwave circulators [76], which may be useful for scalable quantum information processing [20]. Recently, AB-stacked MoTe<sub>2</sub>/WSe<sub>2</sub>, which hosts a magnetic Chern insulator at a carrier density of one hole per moiré superlattice site, has been shown to demonstrate intrinsic spin- or valley-Hall torques that lead to magnetization switching with a current density smaller than 10<sup>3</sup> A/cm<sup>2</sup>. These results suggest that even moiré systems that are not graphene-based form an attractive system for the efficient electrical control of magnetism [77]. The giant unidirectional magnetoresistance (UMR) seen in TBG can be utilized for diode-like current rectification and can convert radiation (e.g., terahertz radiation) into currents for energy harvesting and photodetection. Thus, the discovery of orbital magnetization in moiré systems has significant potential for technological applications. The realization of this potential will require overcoming a variety of challenges. A significant challenge is the development of large-scale fabrication techniques in which the relative alignment or twist angle between layers can be reliably reproduced with an angular precision below 0.1 degrees [46]. In addition, new techniques for spectroscopic readout must be developed as conventional techniques such as neutron spectroscopy do not perform well on 2D materials. This is because conventional methods produce signals that are proportional to the volume of the material sample [11]. Additionally, obtaining robust orbital magnetization at room temperature is a significant challenge for these moiré systems. Future research directions include further examinations of orbital magnetization beyond graphene-based moiré systems, a better understanding of the mechanism and dynamics for the switching of magnetization and a detailed study of domain structures such as magnetic domain walls in these moiré systems [73].

**Author Contributions:** Conceptualization, P.J.; data curation, P.J.; writing—original draft preparation, P.J.; writing—review and editing, B.S.; funding acquisition, B.S. All authors have read and agreed to the published version of the manuscript.

**Funding:** This research was funded by IMEC.

**Institutional Review Board Statement:** Not applicable.

**Informed Consent Statement:** Not applicable.

**Data Availability Statement:** Not applicable.

**Conflicts of Interest:** The authors declare no conflict of interest.

## References

1. Li, G.; Luican, A.; dos Santos, J.M.B.L.; Neto, A.H.C.; Reina, A.; Kong, J.; Andrei, E.Y. Observation of Van Hove singularities in twisted graphene layers. *Nat. Phys.* **2010**, *6*, 109–113. [[CrossRef](#)]
2. Kim, K.; Yankowitz, M.; Fallahzad, B.; Kang, S.; Movva, H.C.P.; Huang, S.; Larentis, S.; Corbet, C.M.; Taniguchi, T.; Watanabe, K.; et al. van der Waals Heterostructures with High Accuracy Rotational Alignment. *Nano Lett.* **2016**, *16*, 1989–1995. [[CrossRef](#)] [[PubMed](#)]
3. Bistritzer, R.; MacDonald, A.H. Moiré bands in twisted double-layer graphene. *Proc. Natl. Acad. Sci. USA* **2011**, *108*, 12233–12237. [[CrossRef](#)] [[PubMed](#)]
4. Fang, S.; Kaxiras, E. Electronic structure theory of weakly interacting bilayers. *Phys. Rev. B* **2016**, *93*, 235153. [[CrossRef](#)]
5. Nam, N.N.T.; Koshino, M. Lattice relaxation and energy band modulation in twisted bilayer graphene. *Phys. Rev. B* **2017**, *96*, 075311. [[CrossRef](#)]
6. Koshino, M.; Yuan, N.F.Q.; Koretsune, T.; Ochi, M.; Kuroki, K.; Fu, L. Maximally Localized Wannier Orbitals and the Extended Hubbard Model for Twisted Bilayer Graphene. *Phys. Rev. X* **2018**, *8*, 031087. [[CrossRef](#)]
7. Cao, Y.; Fatemi, V.; Demir, A.; Fang, S.; Tomarken, S.L.; Luo, J.Y.; Sanchez-Yamagishi, J.D.; Watanabe, K.; Taniguchi, T.; Kaxiras, E.; et al. Correlated insulator behaviour at half-filling in magic-angle graphene superlattices. *Nature* **2018**, *556*, 80–84. [[CrossRef](#)] [[PubMed](#)]

8. Cao, Y.; Fatemi, V.; Fang, S.; Watanabe, K.; Taniguchi, T.; Kaxiras, E.; Jarillo-Herrero, P. Unconventional superconductivity in magic-angle graphene superlattices. *Nature* **2018**, *556*, 43–50. [[CrossRef](#)]
9. Sharpe, A.L.; Fox, E.J.; Barnard, A.W.; Finney, J.; Watanabe, K.; Taniguchi, T.; Kastner, M.A.; Goldhaber-Gordon, D. Emergent ferromagnetism near three-quarters filling in twisted bilayer graphene. *Science* **2019**, *365*, 605–608. [[CrossRef](#)]
10. Xian, L.; Claassen, M.; Kiese, D.; Scherer, M.M.; Trebst, S.; Kennes, D.M.; Rubio, A. Realization of nearly dispersionless bands with strong orbital anisotropy from destructive interference in twisted bilayer MoS<sub>2</sub>. *Nat. Commun.* **2021**, *12*, 5644. [[CrossRef](#)]
11. Kennes, D.M.; Claassen, M.; Xian, L.; Georges, A.; Millis, A.J.; Hone, J.; Dean, C.R.; Basov, D.N.; Pasupathy, A.N.; Rubio, A. Moiré heterostructures as a condensed-matter quantum simulator. *Nat. Phys.* **2021**, *17*, 155–163. [[CrossRef](#)]
12. Wang, L.; Shih, E.-M.; Ghiotto, A.; Xian, L.; Rhodes, D.A.; Tan, C.; Claassen, M.; Kennes, D.M.; Bai, Y.; Kim, B.; et al. Correlated electronic phases in twisted bilayer transition metal dichalcogenides. *Nat. Mater.* **2020**, *19*, 861–866. [[CrossRef](#)]
13. Shimazaki, Y.; Schwartz, I.; Watanabe, K.; Taniguchi, T.; Kroner, M.; Imamoğlu, A. Strongly correlated electrons and hybrid excitons in a moiré heterostructure. *Nature* **2020**, *580*, 472–477. [[CrossRef](#)] [[PubMed](#)]
14. Tran, K.; Moody, G.; Wu, F.; Lu, X.; Choi, J.; Kim, K.; Rai, A.; Sanchez, D.A.; Quan, J.; Singh, A.; et al. Evidence for moiré excitons in van der Waals heterostructures. *Nature* **2019**, *567*, 71–75. [[CrossRef](#)] [[PubMed](#)]
15. Regan, E.C.; Wang, D.; Jin, C.; Utama, M.I.B.; Gao, B.; Wei, X.; Zhao, S.; Zhao, W.; Zhang, Z.; Yumigeta, K.; et al. Mott and generalized Wigner crystal states in WSe<sub>2</sub>/WS<sub>2</sub> moiré superlattices. *Nature* **2020**, *579*, 359–363. [[CrossRef](#)]
16. Liu, X.; Hao, Z.; Khalaf, E.; Lee, J.Y.; Ronen, Y.; Yoo, H.; Najafabadi, D.H.; Watanabe, K.; Taniguchi, T.; Vishwanath, A.; et al. Tunable spin-polarized correlated states in twisted double bilayer graphene. *Nature* **2020**, *583*, 221–225. [[CrossRef](#)]
17. Shen, C.; Chu, Y.; Wu, Q.; Li, N.; Wang, S.; Zhao, Y.; Tang, J.; Liu, J.; Tian, J.; Watanabe, K.; et al. Correlated states in twisted double bilayer graphene. *Nat. Phys.* **2020**, *16*, 520–525. [[CrossRef](#)]
18. Chen, G.; Sharpe, A.L.; Fox, E.J.; Zhang, Y.-H.; Wang, S.; Jiang, L.; Lyu, B.; Li, H.; Watanabe, K.; Taniguchi, T.; et al. Tunable correlated Chern insulator and ferromagnetism in a moiré superlattice. *Nature* **2020**, *579*, 56–61. [[CrossRef](#)]
19. Chen, G.; Sharpe, A.L.; Fox, E.J.; Wang, S.; Lyu, B.; Jiang, L.; Li, H.; Watanabe, K.; Taniguchi, T.; Crommie, M.F.; et al. Tunable Orbital Ferromagnetism at Noninteger Filling of a Moiré Superlattice. *Nano Lett.* **2022**, *22*, 238–245. [[CrossRef](#)]
20. Polshyn, H.; Zhu, J.; Kumar, M.A.; Zhang, Y.; Yang, F.; Tschirhart, C.L.; Serlin, M.; Watanabe, K.; Taniguchi, T.; MacDonald, A.H.; et al. Electrical switching of magnetic order in an orbital Chern insulator. *Nature* **2020**, *588*, 66–70. [[CrossRef](#)]
21. Sharpe, A.L.; Fox, E.J.; Barnard, A.W.; Finney, J.; Watanabe, K.; Taniguchi, T.; Kastner, M.A.; Goldhaber-Gordon, D. Evidence of Orbital Ferromagnetism in Twisted Bilayer Graphene Aligned to Hexagonal Boron Nitride. *Nano Lett.* **2021**, *21*, 4299–4304. [[CrossRef](#)] [[PubMed](#)]
22. Tschirhart, C.L.; Serlin, M.; Polshyn, H.; Shragai, A.; Xia, Z.; Zhu, J.; Zhang, Y.; Watanabe, K.; Taniguchi, T.; Huber, M.E.; et al. Imaging orbital ferromagnetism in a moiré Chern insulator. *Science* **2021**, *372*, 1323–1327. [[CrossRef](#)] [[PubMed](#)]
23. Yankowitz, M.; Chen, S.; Polshyn, H.; Zhang, Y.; Watanabe, K.; Taniguchi, T.; Graf, D.; Young, A.F.; Dean, C.R. Tuning superconductivity in twisted bilayer graphene. *Science* **2019**, *363*, 1059–1064. [[CrossRef](#)]
24. Chen, G.; Jiang, L.; Wu, S.; Lyu, B.; Li, H.; Chittari, B.L.; Watanabe, K.; Taniguchi, T.; Shi, Z.; Jung, J.; et al. Evidence of a gate-tunable Mott insulator in a trilayer graphene moiré superlattice. *Nat. Phys.* **2019**, *15*, 237–241. [[CrossRef](#)]
25. Chen, G.; Sharpe, A.L.; Gallagher, P.; Rosen, I.T.; Fox, E.J.; Jiang, L.; Lyu, B.; Li, H.; Watanabe, K.; Taniguchi, T.; et al. Signatures of tunable superconductivity in a trilayer graphene moiré superlattice. *Nature* **2019**, *572*, 215–219. [[CrossRef](#)] [[PubMed](#)]
26. Cao, Y.; Rodan-Legrain, D.; Rubies-Bigorda, O.; Park, J.M.; Watanabe, K.; Taniguchi, T.; Jarillo-Herrero, P. Tunable correlated states and spin-polarized phases in twisted bilayer-bilayer graphene. *Nature* **2020**, *583*, 215–220. [[CrossRef](#)]
27. Burg, G.W.; Zhu, J.; Taniguchi, T.; Watanabe, K.; MacDonald, A.H.; Tutuc, E. Correlated Insulating States in Twisted Double Bilayer Graphene. *Phys. Rev. Lett.* **2019**, *123*, 197702. [[CrossRef](#)]
28. de Vries, F.K.; Zhu, J.; Portolés, E.; Zheng, G.; Masseroni, M.; Kurzman, A.; Taniguchi, T.; Watanabe, K.; MacDonald, A.H.; Ensslin, K.; et al. Combined Minivalley and Layer Control in Twisted Double Bilayer Graphene. *Phys. Rev. Lett.* **2020**, *125*, 176801. [[CrossRef](#)]
29. He, M.; Li, Y.; Cai, J.; Liu, Y.; Watanabe, K.; Taniguchi, T.; Xu, X.; Yankowitz, M. Symmetry breaking in twisted double bilayer graphene. *Nat. Phys.* **2020**, *17*, 26–30. [[CrossRef](#)]
30. Song, Z.; Wang, Z.; Shi, W.; Li, G.; Fang, C.; Bernevig, B.A. All Magic Angles in Twisted Bilayer Graphene are Topological. *Phys. Rev. Lett.* **2019**, *123*, 036401. [[CrossRef](#)]
31. Po, H.C.; Zou, L.; Senthil, T.; Vishwanath, A. Faithful tight-binding models and fragile topology of magic-angle bilayer graphene. *Phys. Rev. B* **2019**, *99*, 195455. [[CrossRef](#)]
32. Herzog-Arbeitman, J.; Song, Z.-D.; Regnault, N.; Bernevig, B.A. Hofstadter Topology: Noncrystalline Topological Materials at High Flux. *Phys. Rev. Lett.* **2020**, *125*, 236804. [[CrossRef](#)] [[PubMed](#)]
33. Lian, B.; Xie, F.; Bernevig, B.A. Landau level of fragile topology. *Phys. Rev. B* **2020**, *102*, 041402. [[CrossRef](#)]
34. Haldane, F.D.M. Model for a Quantum Hall Effect without Landau Levels: Condensed-Matter Realization of the “Parity Anomaly”. *Phys. Rev. Lett.* **1988**, *61*, 2015–2018. [[CrossRef](#)] [[PubMed](#)]
35. Zhang, Y.-H.; Mao, D.; Cao, Y.; Jarillo-Herrero, P.; Senthil, T. Nearly flat Chern bands in moiré superlattices. *Phys. Rev. B* **2019**, *99*, 075127. [[CrossRef](#)]
36. Liu, J.; Ma, Z.; Gao, J.; Dai, X. Quantum Valley Hall Effect, Orbital Magnetism, and Anomalous Hall Effect in Twisted Multilayer Graphene Systems. *Phys. Rev. X* **2019**, *9*, 031021. [[CrossRef](#)]

37. Serlin, M.; Tschirhart, C.L.; Polshyn, H.; Zhang, Y.; Zhu, J.; Watanabe, K.; Taniguchi, T.; Balents, L.; Young, A.F. Intrinsic quantized anomalous Hall effect in a moiré heterostructure. *Science* **2020**, *367*, 900–903. [[CrossRef](#)]
38. Bultinck, N.; Chatterjee, S.; Zaletel, M.P. Mechanism for Anomalous Hall Ferromagnetism in Twisted Bilayer Graphene. *Phys. Rev. Lett.* **2020**, *124*, 166601. [[CrossRef](#)]
39. Zhang, Y.-H.; Mao, D.; Senthil, T. Twisted bilayer graphene aligned with hexagonal boron nitride: Anomalous Hall effect and a lattice model. *Phys. Rev. Res.* **2019**, *1*, 033126. [[CrossRef](#)]
40. Liu, J.; Dai, X. Theories for the correlated insulating states and quantum anomalous Hall effect phenomena in twisted bilayer graphene. *Phys. Rev. B* **2021**, *103*, 035427. [[CrossRef](#)]
41. Wu, F.; Das Sarma, S. Collective Excitations of Quantum Anomalous Hall Ferromagnets in Twisted Bilayer Graphene. *Phys. Rev. Lett.* **2020**, *124*, 046403. [[CrossRef](#)]
42. Chatterjee, S.; Bultinck, N.; Zaletel, M.P. Symmetry breaking and skyrmionic transport in twisted bilayer graphene. *Phys. Rev. B* **2020**, *101*, 165141. [[CrossRef](#)]
43. Repellin, C.; Dong, Z.; Zhang, Y.-H.; Senthil, T. Ferromagnetism in Narrow Bands of Moiré Superlattices. *Phys. Rev. Lett.* **2020**, *124*, 187601. [[CrossRef](#)] [[PubMed](#)]
44. Alavirad, Y.; Sau, J. Ferromagnetism and its stability from the one-magnon spectrum in twisted bilayer graphene. *Phys. Rev. B* **2020**, *102*, 235123. [[CrossRef](#)]
45. Chen, S.; He, M.; Zhang, Y.-H.; Hsieh, V.; Fei, Z.; Watanabe, K.; Taniguchi, T.; Cobden, D.H.; Xu, X.; Dean, C.R.; et al. Electrically tunable correlated and topological states in twisted monolayer–bilayer graphene. *Nat. Phys.* **2021**, *17*, 374–380. [[CrossRef](#)]
46. Lau, C.N.; Bockrath, M.W.; Mak, K.F.; Zhang, F. Reproducibility in the fabrication and physics of moiré materials. *Nature* **2022**, *602*, 41–50. [[CrossRef](#)]
47. Andrei, E.Y.; Efetov, D.K.; Jarillo-Herrero, P.; MacDonald, A.H.; Mak, K.F.; Senthil, T.; Tutuc, E.; Yazdani, A.; Young, A.F. The marvels of moiré materials. *Nat. Rev. Mater.* **2021**, *6*, 201–206. [[CrossRef](#)]
48. He, F.; Zhou, Y.; Ye, Z.; Cho, S.-H.; Jeong, J.; Meng, X.; Wang, Y. Moiré Patterns in 2D Materials: A Review. *ACS Nano* **2021**, *15*, 5944–5958. [[CrossRef](#)]
49. Shi, B.; Qi, P.; Jiang, M.; Dai, Y.; Lin, F.; Zhang, H.; Fang, Z. Exotic physical properties of 2D materials modulated by moiré superlattices. *Mater. Adv.* **2021**, *2*, 5542–5559. [[CrossRef](#)]
50. Xiao, D.; Chang, M.-C.; Niu, Q. Berry phase effects on electronic properties. *Rev. Mod. Phys.* **2010**, *82*, 1959–2007. [[CrossRef](#)]
51. Xie, M.; MacDonald, A.H. Nature of the Correlated Insulator States in Twisted Bilayer Graphene. *Phys. Rev. Lett.* **2020**, *124*, 097601. [[CrossRef](#)] [[PubMed](#)]
52. Hanke, J.-P.; Freimuth, F.; Nandy, A.K.; Zhang, H.; Blügel, S.; Mokrousov, Y. Role of Berry phase theory for describing orbital magnetism: From magnetic heterostructures to topological orbital ferromagnets. *Phys. Rev. B* **2016**, *94*, 121114. [[CrossRef](#)]
53. Zhu, J.; Su, J.-J.; MacDonald, A.H. Voltage-Controlled Magnetic Reversal in Orbital Chern Insulators. *Phys. Rev. Lett.* **2020**, *125*, 227702. [[CrossRef](#)]
54. Resta, R. Electrical polarization and orbital magnetization: The modern theories. *J. Phys. Condens. Matter* **2010**, *22*, 123201. [[CrossRef](#)]
55. Meyer, A.J.P.; Asch, G. Experimental  $g'$  and  $g$  Values of Fe, Co, Ni, and Their Alloys. *J. Appl. Phys.* **1961**, *32*, S330–S333. [[CrossRef](#)]
56. Thole, B.T.; Carra, P.; Sette, F.; van der Laan, G. X-ray circular dichroism as a probe of orbital magnetization. *Phys. Rev. Lett.* **1992**, *68*, 1943–1946. [[CrossRef](#)]
57. Oh, Y.-W.; Baek, S.-H.C.; Kim, Y.M.; Lee, H.Y.; Lee, K.-D.; Yang, C.-G.; Park, E.-S.; Lee, K.-S.; Kim, K.-W.; Go, G.; et al. Field-free switching of perpendicular magnetization through spin–orbit torque in antiferromagnet/ferromagnet/oxide structures. *Nat. Nanotechnol.* **2016**, *11*, 878–884. [[CrossRef](#)]
58. He, W.-Y.; Goldhaber-Gordon, D.; Law, K.T. Giant orbital magnetoelectric effect and current-induced magnetization switching in twisted bilayer graphene. *Nat. Commun.* **2020**, *11*, 1650. [[CrossRef](#)]
59. Li, S.-Y.; Zhang, Y.; Ren, Y.-N.; Liu, J.; Dai, X.; He, L. Experimental evidence for orbital magnetic moments generated by moiré-scale current loops in twisted bilayer graphene. *Phys. Rev. B* **2020**, *102*, 121406. [[CrossRef](#)]
60. Chittari, B.L.; Chen, G.; Zhang, Y.; Wang, F.; Jung, J. Gate-Tunable Topological Flat Bands in Trilayer Graphene Boron-Nitride Moiré Superlattices. *Phys. Rev. Lett.* **2019**, *122*, 016401. [[CrossRef](#)] [[PubMed](#)]
61. He, M.; Zhang, Y.-H.; Li, Y.; Fei, Z.; Watanabe, K.; Taniguchi, T.; Xu, X.; Yankowitz, M. Competing correlated states and abundant orbital magnetism in twisted monolayer-bilayer graphene. *Nat. Commun.* **2021**, *12*, 4727. [[CrossRef](#)] [[PubMed](#)]
62. Matsukura, F.; Tokura, Y.; Ohno, H. Control of magnetism by electric fields. *Nat. Nanotechnol.* **2015**, *10*, 209–220. [[CrossRef](#)] [[PubMed](#)]
63. Chiba, D.; Werpachowska, A.; Endo, M.; Nishitani, Y.; Matsukura, F.; Dietl, T.; Ohno, H. Anomalous Hall Effect in Field-Effect Structures of (Ga,Mn)As. *Phys. Rev. Lett.* **2010**, *104*, 106601. [[CrossRef](#)] [[PubMed](#)]
64. Zhang, S.; Wang, R.; Wang, X.; Wei, B.; Chen, B.; Wang, H.; Shi, G.; Wang, F.; Jia, B.; Ouyang, Y.; et al. Experimental Observation of the Gate-Controlled Reversal of the Anomalous Hall Effect in the Intrinsic Magnetic Topological Insulator  $\text{MnBi}_2\text{Te}_4$  Device. *Nano Lett.* **2019**, *20*, 709–714. [[CrossRef](#)]
65. Zhang, Y.-H.; Senthil, T. Quantum Hall spin liquids and their possible realization in moiré systems. *Phys. Rev. B* **2020**, *102*, 115127. [[CrossRef](#)]

66. Repellin, C.; Senthil, T. Chern bands of twisted bilayer graphene: Fractional Chern insulators and spin phase transition. *Phys. Rev. Res.* **2020**, *2*, 023238. [[CrossRef](#)]
67. Liu, J.; Liu, J.; Dai, X. Pseudo Landau level representation of twisted bilayer graphene: Band topology and implications on the correlated insulating phase. *Phys. Rev. B* **2019**, *99*, 155415. [[CrossRef](#)]
68. Lopez-Bezanilla, A. Emergence of flat-band magnetism and half-metallicity in twisted bilayer graphene. *Phys. Rev. Mater.* **2019**, *3*, 054003. [[CrossRef](#)]
69. Huang, C.; Wei, N.; MacDonald, A.H. Current-Driven Magnetization Reversal in Orbital Chern Insulators. *Phys. Rev. Lett.* **2021**, *126*, 056801. [[CrossRef](#)]
70. Yue, K.; Liu, Y.; Lake, R.K.; Parker, A.C. A brain-plausible neuromorphic on-the-fly learning system implemented with magnetic domain wall analog memristors. *Sci. Adv.* **2019**, *5*, eaau8170. [[CrossRef](#)]
71. Jiang, M.; Asahara, H.; Sato, S.; Kanaki, T.; Yamasaki, H.; Ohya, S.; Tanaka, M. Efficient full spin-orbit torque switching in a single layer of a perpendicularly magnetized single-crystalline ferromagnet. *Nat. Commun.* **2019**, *10*, 2590. [[CrossRef](#)] [[PubMed](#)]
72. Fan, Y.; Upadhyaya, P.; Kou, X.; Lang, M.; Takei, S.; Wang, Z.; Tang, J.; He, L.; Chang, L.-T.; Montazeri, M.; et al. Magnetization switching through giant spin-orbit torque in a magnetically doped topological insulator heterostructure. *Nat. Mater.* **2014**, *13*, 699–704. [[CrossRef](#)] [[PubMed](#)]
73. Tschirhart, C.L.; Redekop, E.; Li, L.; Li, T.; Jiang, S.; Arp, T.; Sheekey, O.; Taniguchi, T.; Watanabe, K.; Huber, M.E.; et al. Intrinsic spin Hall torque in a moiré Chern magnet. *Nat. Phys.* **2023**, *19*, 807–813. [[CrossRef](#)]
74. Tong, Q.; Liu, F.; Xiao, J.; Yao, W. Skyrmions in the Moiré of van der Waals 2D Magnets. *Nano Lett.* **2018**, *18*, 7194–7199. [[CrossRef](#)]
75. Jadaun, P.; Cui, C.; Liu, S.; Incorvia, J.A.C. Adaptive cognition implemented with a context-aware and flexible neuron for next-generation artificial intelligence. *PNAS Nexus* **2022**, *1*, pgac206. [[CrossRef](#)]
76. Viola, G.; DiVincenzo, D.P. Hall Effect Gyrotors and Circulators. *Phys. Rev. X* **2014**, *4*, 021019. [[CrossRef](#)]
77. Liu, Y.; Holder, T.; Yan, B. Chirality-Induced Giant Unidirectional Magnetoresistance in Twisted Bilayer Graphene. *Innovation* **2021**, *2*, 100085. [[CrossRef](#)]

**Disclaimer/Publisher’s Note:** The statements, opinions and data contained in all publications are solely those of the individual author(s) and contributor(s) and not of MDPI and/or the editor(s). MDPI and/or the editor(s) disclaim responsibility for any injury to people or property resulting from any ideas, methods, instructions or products referred to in the content.